ORIGINAL ARTICLE

CIWEM Chartered Institution of Water and Environmental Management Journal of Flood Risk Management WILEY

Delineation of flood-prone areas in cliffed coastal regions through a procedure based on the geomorphic flood index

Cinzia Albertini[1,2] | Domenico Miglino[2] | Vito Iacobellis[3] |
Francesco De Paola[2] | Salvatore Manfreda[2]

[1]Dipartimento di Scienze Agro Ambientali e Territoriali (DISAAT), Università degli Studi di Bari Aldo Moro, Bari, Italy

[2]Dipartimento di Ingegneria Civile, Edile e Ambientale (DICEA), Università di Napoli Federico II, Naples, Italy

[3]Dipartimento di Ingegneria Civile, Ambientale, del Territorio, Edile e di Chimica (DICATECh), Politecnico di Bari, Bari, Italy

Correspondence
Cinzia Albertini, Dipartimento di Scienze Agro Ambientali e Territoriali (DISAAT), Università degli Studi di Bari Aldo Moro, 70126 Bari, Italy.
Email: cinzia.albertini@uniba.it

Funding information
Research agreement between the Italian Ministry of Environment, Land and Sea and DICEA.

Abstract

The geomorphic flood index (GFI) method provides a good representation of flood-prone areas. However, the method does not account for floodwater transfers in undefined interbasins (UIBs), which represent intercluded small basins along the coastline likely to be flooded by adjacent major rivers. The present work addresses this shortcoming by complementing the GFI approach with an iterative procedure that considers UIBs and water transfers between basins. The methodology was tested on a coastal basin in southern Italy and the outcome was compared with a flood map obtained by a two-dimensional hydraulic simulation. GFI performance as a morphological descriptor improved from 74% (standard method) to 94% with the addition of the iterative procedure. The proposed methodology, with the same parameterization, was applied on a second adjacent coastal basin obtaining improvements both in terms of true positive (from 56 to 79%) and false negative rates (from 44 to 21%). Finally, a sensitivity analysis to the flood return periods highlighted a strong influence on model parameterization for return periods below 20 years. This achievement represents a new development in the application of the GFI method, which can help stakeholders in a more time- and cost-effective flood risk management in hazard-prone areas.

KEYWORDS
coastal flood susceptibility, digital elevation model, flood risk, geomorphic flood index

1 | INTRODUCTION

Floods are the most devastating water-related natural hazards affecting about 2 billion people worldwide in the last 20 years (Wallemacq, 2018). Moreover, the frequency and magnitude of river floods may increase globally due to changing rainfall and runoff (Alfieri et al., 2017; Blöschl et al., 2007; Hirabayashi et al., 2013; Solomon et al., 2007; Wagener et al., 2010). In this context, human-induced hydrologic changes (Di Baldassarre et al., 2015, 2017; Wagener et al., 2010) can lead to increased flood damages exacerbated by higher land use and population density in flood-prone areas (Jonkman, 2005; Merz et al., 2010).

Coastal zones are the most densely inhabited areas characterized by great social and economic development

(Bates et al., 2005; Neumann et al., 2015) and a wide range of morphologies, including flat terrain, smooth hills, rocky headlands and bedrock cliffs. For instance, several examples of rocky coastlands can be found along the Tyrrhenian coast in Italy (e.g., Campania, Calabria, Liguria, and Toscana). According to the definition given in Violante (2009), rocky coasts include steep coastal watersheds, fan-delta systems and torrential ephemeral rivers, characterized by periods of apparent stability and commonly poorly monitored, diverted or covered for urban development. In these settings, detecting areas exposed to floods is of paramount importance for preventing human and economic losses, considering the high hazard potential of extreme hydrological events and the occurrence of interbasin water transfers.

Traditional flood hazard assessment relies on hydrologic and hydraulic simulation models, which requires records of observed river discharges at gauging stations (Nardi et al., 2006; Samela et al., 2018). However, numerical simulations can be computationally demanding and can require a large amount of data for validation and the calibration of parameters to fully describe the flow dynamics (Bates, 2004; Manfreda et al., 2014). Hydrological and hydraulic studies are frequently limited by data availability, especially in small and ungauged basins, thus making it difficult to assess hazard.

In the last few years, new simplified methods and tools for mapping flood-prone areas based on digital elevation models (DEMs) have been established (Manfreda et al., 2014; Samela et al., 2017, 2018; Tavares da Costa et al., 2019, 2020). They rely on topographic and hydrogeomorphic properties of river basins. For instance, Nobre et al. (2016) developed a flood mapping method based on a height above the nearest drainage (HAND) contour map drawn by connecting points with the same vertical distance to the nearest river channel and associating a flood hazard rank. Moreover, different geomorphic classifiers, such as the HAND, have been proposed. Manfreda et al. (2008) adopted a generalized version of the topographic index by Kirkby (1975), called modified topographic index (TI_m), for deriving flood extent maps using a calibrated threshold that discriminates between flooded and non-flooded areas. Degiorgis et al. (2012) proposed a threshold binary classifier based on several DEM-derived quantitative morphologic features. Nardi et al. (2006) implemented a hydrogeomorphic method linking a simplified flood relation with the geomorphic properties of the river basin.

These methods and tools enable a preliminary flood hazard assessment over large areas even when data are limited, highlighting the potential of terrain morphology alone as a key information source. Based on this finding,

Samela et al. (2017) compared performances of 11 flood-related morphological descriptors. In particular, the authors analyzed five single features (i.e., upslope contributing area, local slope, surface curvature, flow distance, and elevation difference to the nearest stream) and four composite indexes, including the modified topographic index and the geomorphic flood index (GFI), which was assessed as the best performing classifier.

The GFI proved to be suitable for large-scale analysis in data-scarce regions (Albano et al., 2020; Samela et al., 2016), as well as a valuable estimate of flood depth that can be used for quantifying flood damages (Manfreda & Samela, 2019). It was successfully applied to several case studies, including applications to basins in the United States (Samela et al., 2017), in Europe (Albano et al., 2020; Manfreda & Samela, 2019; Samela et al., 2018; Tavares da Costa et al., 2019), and Africa (Samela et al., 2016). However, none of these works focused on coastal river basins and accounted for the difficulties in the extraction of the river network in low-lying areas, nor for the possibility of water transfers across basins. DEM-based procedures, such as the GFI method, strongly depend on the elevation difference to the nearest channel (or HAND, Nobre et al., 2016) and a correct identification of the river network. These dependencies can affect the accuracy of results, especially in flat areas, where low spatial resolution and difficulties in extracting flow paths are often found (Tavares da Costa et al., 2019). This "flat area issue" (Nardi et al., 2008; Petroselli & Alvarez, 2012) indeed arises due to zero-slope areas and prevents the identification of a continuous channel network or the calculation of geomorphic indexes. Moreover, the GFI is usually computed at the basin scale and its definition is constrained to the basin boundaries, which limit water transfers even if differences in elevation and slope between two adjacent basins allow it. These issues are especially found along cliffed coastal areas often characterized by adjacent river basins draining to the sea, separated by smaller interbasins whose flood hazard is triggered by large-magnitude flood events that occur in the adjacent ones. A river network is often undefined in interbasins or difficult to identify using traditional criteria for river network identification (e.g., the area-slope criterion proposed by Giannoni et al., 2005), denying any possibility to calculate the GFI and delineate flood-prone areas. Hereinafter, these areas are referred to as undefined interbasins (UIBs).

In this work, interbasin transfers of floodwater are incorporated in the GFI method to account for UIBs. The aim is to provide a methodology to map flood-prone areas in cliffed coastal regions characterized by UIBs, considering the interconnection of the flow between adjacent

basins. The method is based on the extrapolation of flood depths at the basin boundaries and the propagation in the adjacent UIBs. In this way, an artificial river network generated by the transfer of floodwater from the main river basin to the adjacent UIBs is defined, which enables the calculation of the GFI and the delineation of flood-prone areas. A coastal basin in the Campania region, southern Italy, is used as a case study and an adjacent basin is used to test the transferability of the procedure in a similar geomorphic context. Flood maps obtained by two-dimensional (2D) hydraulic simulations for a return period of 300 years are used to assess the skill of the proposed approach. Finally, the sensitivity of the method to the return period is investigated.

This article is organized in the following way. Section 2 introduces the case study areas selected for testing and validating the methodology. Section 3 gives an overview of the general workflow to apply the GFI and describes the method to extend the calculation to the UIBs. Furthermore, details about the hydraulic model and sensitivity analysis are given. Section 4 presents the results of the proposed approach in the test and validation river basins and in Section 5 main findings are discussed. Finally, in Section 6, conclusions are presented.

2 | STUDY AREAS

The proposed methodology was applied to two case studies located in Castellammare di Stabia, Campania region (southern Italy) (Figure 1). The urban area of Castellammare, similarly to many other rocky coastal zones of the Sorrentine Peninsula and Amalfi coast, mainly extends on active alluvial fans (Santo et al., 2002) and it is crossed by torrential watercourses often canalized due to urban development (Pennetta, 2009). This region is characterized by heavy convective precipitation with mean annual values between 1000 and 2000 mm (Vennari et al., 2016). These features make this territory highly vulnerable to flooding, especially to flash floods (Santo et al., 2015), a consequence of the high slopes but also the short concentration time that characterize small river basins in the Southern Apennines. Vennari et al. (2016) built a detailed database on flash flood events that occurred in the Campania region between 1540 and 2015 and reported around 10 devastating flood events recorded in Castellammare di Stabia since 1931. Santo et al. (2002) investigated flood hazard in Castellammare di Stabia by reviewing historical events, including the flash floods occurred in August 1935, November 1987, and October 2000.
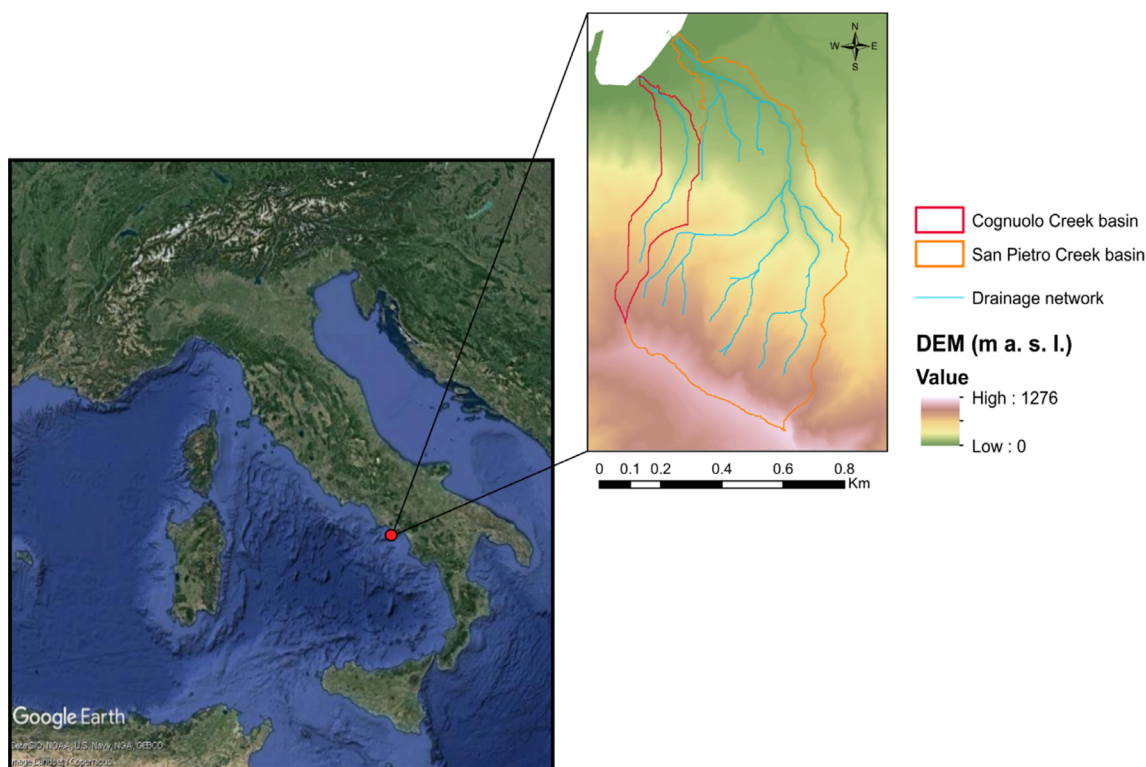

FIGURE 1   Location of the study area and digital elevation model (DEM) with a 5-m resolution. The two coastal basins identified for the analyses are located in the Campania region, southern Italy (map source: Google, SIO, NCAA, US Navy, NGA, GEBCO, Landsat)

Several torrential streams that originate from the northern part of the Lattari Mts and flow into the Tyrrhenian Sea in the Gulf of Castellammare di Stabia are present in the study area. These include the San Pietro Creek, which was selected as a test catchment for the new methodology, and the adjacent Cognuolo Creek, which was selected for validation purposes.

The San Pietro Creek basin is characterized by a drainage area of about 3.5 km^2 and an average slope of about 80%, while the Cognuolo Creek basin has a drainage area of about 0.5 km^2 and an average slope of about 63%. The mean altitude of the San Pietro Creek and Cognuolo Creek basins is about 661 and 617 m, respectively (Santo et al., 2002).

3 | METHODOLOGY

The GFI method is complemented by an iteration procedure to enhance its ability in delineating flooded areas in UIBs in cliffed coastal regions. A complete overview of the methodological workflow is shown in Figure 2. Starting from the computation of the GFI, a threshold binary classification (Degiorgis et al., 2012, 2013) is carried out to discriminate between flooded and non-flooded areas comparing results with the reference flood maps obtained from the 2D hydraulic simulations. Whenever the coastal zone is characterized by UIBs, an iteration procedure based on the extraction of the geomorphic flood depth, WD, at the watershed divide is applied.

3.1 | The GFI

The proposed methodology to identify flood-prone areas in coastal zones is based on the GFI and its ability to discriminate between flooded and non-flooded areas through its use as a threshold binary classifier (Degiorgis et al., 2012; Samela et al., 2017).

The GFI is defined as the natural logarithm of the ratio between the water level in each cell of the river network, h_r (m), and the difference in elevation, H (m) (or HAND, Nobre et al., 2016), between any location of the basin and the nearest element of the river network identified following the flow path:

$$\mathrm{GFI} = \ln\left(\frac{h_r}{H}\right) \qquad (1)$$

The variable h_r in Equation (1) is derived from a hydraulic scaling relationship proposed by Leopold and Maddock (1953) and further investigated by Nardi et al. (2006):
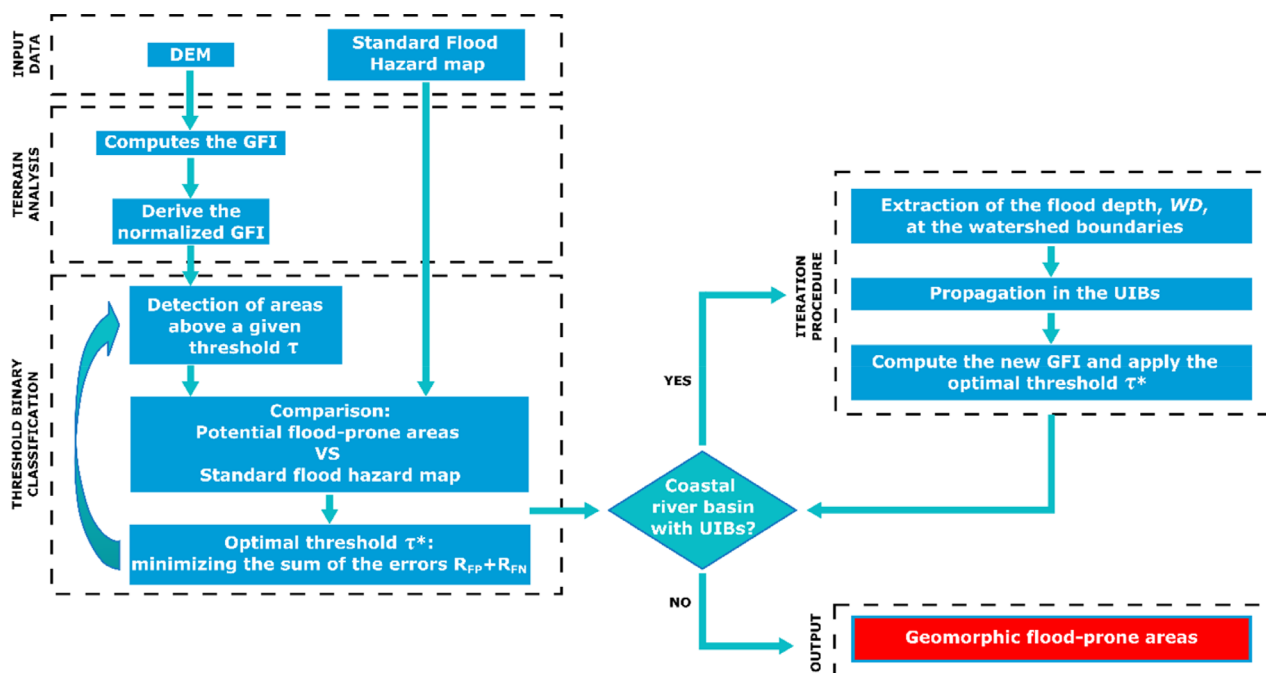
$$h_r \approx a \cdot A_r^n \qquad (2)$$

FIGURE 2 Methodological workflow for flood-prone areas delineation using the geomorphic flood index (GFI) method integrated with the iteration procedure in the coastal undefined interbasins (UIBs)

where a is a scale factor, A_r (km^2) is the upslope contributing area, and n is a dimensionless exponent. To assign values to the parameters a and n, a calibration process using paired values of h_r and A_r for several gauging stations is needed (Manfreda & Samela, 2019). In cases of low data availability, the parameter a can be set equal to one since it does not influence subsequent delineation of the flood-prone areas with the GFI, while a value of 0.354 estimated as the average among values extracted from literature can be used for the exponent n (see Samela et al., 2018).

3.1.1 | Input data and threshold binary classification

The delineation of flood-prone areas through the GFI method is based on a few steps, briefly described below and illustrated in Figure 2 (left panel). First, the GFI and its constituting layers, that is, H and h_r, need to be computed. To this end, a DEM is required as input data and a preliminary terrain analysis should be performed. In this study, a 5-m resolution DEM provided by the Campania Region was used (see Figure 1). The preprocessing phase is required to identify the river network. Hence, a filled DEM is used to derive the flow direction and flow accumulation matrixes following the well-known D8 algorithm (O'Callaghan & Mark, 1984).

Once the GFI is computed over the basin of interest, it is used in a threshold binary classification to derive a flood hazard map. The GFI values are first normalized in the range $-1{:}1$, then the normalized map is transformed into a binary map of potential flood-prone areas applying a threshold value, τ, that represents a linear boundary (Samela et al., 2017). This classification allows for the separation of points within the basin into two classes, that is, flooded and non-flooded locations, identified by pixels with a normalized GFI value above and below τ, respectively. The threshold is iteratively calibrated by comparing a series of GFI-derived binary maps with a reference flood map obtained from 1D or 2D hydraulic models (see Section 3.3). To calibrate the optimal threshold τ, the reference map needs to cover at least 2% of the investigated basin (Samela et al., 2017). The calibration process involves selecting τ value that minimizes the sum of two performance metrics, namely the false positive rate R_{FP} (overestimation) and the false negative rate R_{FN} (underestimation), assigning equal weights to both errors (Samela et al., 2018). Description of the performance measures of the threshold binary classification is presented in Section 3.1.2.

More recently, Manfreda and Samela (2019) further explored the GFI method and highlighted the potential for a preliminary, but cost-effective, flood hazard assessment through a straightforward estimate of flood depth, WD (m), within the flooded pixels:

$$\mathrm{WD} = h_r - H \tag{3}$$

where h_r can be computed using Equation (2).

In most cases, the parameter a is unknown and set for simplicity to one. In the logarithmic definition of the GFI, the coefficient a represents a known-term producing a simple translation of the function that does not affect the relative distribution of values. The calibrated threshold τ incorporates the coefficient a that can be estimated using the expression provided by Manfreda and Samela (2019):

$$a = \frac{1}{\exp(\tau)} \tag{4}$$

The formula allows for a parametric description of h_r for the estimation of WD that is used to derive the modified version of the GFI (see Section 3.2).

3.1.2 | Performance metrics

In this section, performance measures used to calibrate the optimal threshold, τ, and as validation statistics are briefly introduced (please refer to Samela et al., 2017, for a more detailed description). To compute performance metrics, a reference flood hazard map is required. For this reason, 2D hydraulic models for both the test and validation case studies were developed (see Section 3.3).

In order to calibrate τ, the sum of the overestimation error, R_{FP}, and underestimation error, R_{FN}, should be minimized. The former is defined by comparing the number of pixels marked as non-flooded by the reference flood map with those incorrectly marked as flooded by the GFI, while the latter is defined by comparing the number of flooded pixels in the reference map with those that the method incorrectly marks as non-flooded.

Performances of the calibration process are also measured in terms of true positive rate, R_{TP}, or sensitivity, and true negative rate, R_{TN}, or specificity, which respectively identify the number of pixels correctly marked as flooded and non-flooded by the GFI method compared to the reference map.

The false positive rate and true positive rate are used to draw the Receiver Operating Characteristics (ROC) curve and specifically measure the area under the ROC curve (AUC), values of which range from 0.5 to 1.0, indicating a random and a perfect classifier, respectively. Both the ROC and the AUC are evaluated using a

reference area that includes the basin of interest and the adjacent UIBs.

3.2 | The GFI applied to UIBs

The proposed methodology is based on the GFI complemented by an iteration procedure applied to the UIBs. The aim of the proposed procedure is to hydrologically connect the UIBs to the main river basin by artificially extending the river network. The iteration procedure is based on the steps summarized in Figure 2 (right panel) and conceptually illustrated in Figure 3.

The first step comprises obtaining the parameter τ using the threshold binary classification, as described in Section 3.1. In the second step, WD is calculated within the basin under study using Equations (3) and (4) and the threshold τ. The third step consists of identifying the WD along the watershed divide by selecting the maximum value among the eight adjacent cells. The maximum value is more likely to generate a water transfer, which can take place in any of the directions regardless of the underlining flow direction map. That is because at the basin divide the flow direction does not account for potential water transfers, even if changes in water elevation may be larger than changes in elevation. Values of WD along the divide are then used to propagate floodwater in the UIBs (yellow shaded areas in Figure 3) and alter the map of contributing areas, A_r, taking into

account the water transfer from adjacent basins. This is achieved assuming that only values of WD exceeding the main river capacity contribute to the flow accumulation along the divide and in the surrounding UIBs. The new contributing area is assigned inverting Equation (2):

$$A_r = (\text{WD} \cdot e^\tau)^{\frac{1}{n}} \tag{5}$$

where WD replaces h_r, n is the value of the exponent, and τ is the calibrated threshold. It should be stressed that although Equation (2) is originally formulated for river channel, in our conceptualization, we assumed that, when water flows from one basin to the adjacent one, the cell that is affected by an increase in the water depth is a channelized pixel and, consequently, the hydraulic relation is applicable in that cell. This assumption allowed us to artificially connect the UIBs to the main river basin in order to account for water transfers between adjacent basins in a simplified way and without the need for increasing the number of model parameters. In addition, this allowed qualitatively obtaining a preliminary and good representation of flooded areas in the UIBs, that otherwise would not be mapped.

Another approximation that could be further investigated is the use of a function specifically developed to describe the hydraulic scaling characteristics of channels on the basin divide. In this context, it is worth mentioning that specific functions have also been proposed for
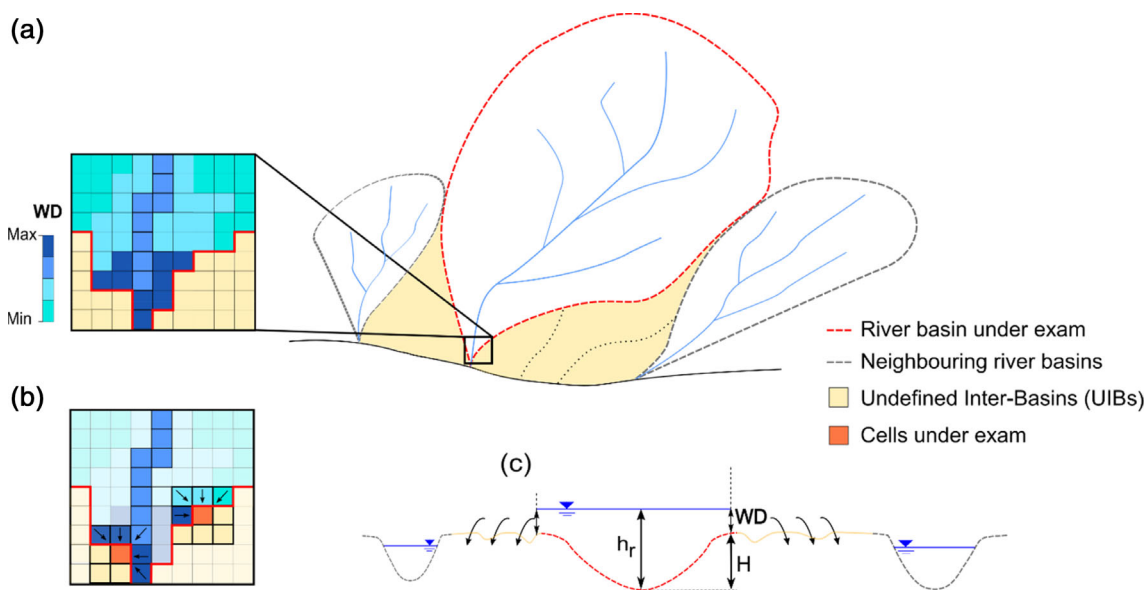

FIGURE 3 A conceptualization of the proposed methodology applied to the undefined interbasins (UIBs) (yellow shaded area) that can be characterized by smaller intercluded UIBs (dotted black lines). (a) Representation of the flood depth, WD, for a portion of the examined basin, computed by geomorphic analysis. (b) In each cell of the UIBs, the maximum value of the flood depth among the adjacent cells is propagated and converted into a new flow accumulation. (c) Schematic representation of a hypothetical section of the study area showing the parameters used in the analyses (water level in the river network, h_r, elevation difference, H, and WD)

floodplains (see Bhowmik, 1984), which could be included that would increase the number of model parameters. Given the nature of the proposed methodology which aims to provide simple and rapid delineation of flood extent, we preferred to use this additional simplifying assumption that also allows deriving the scale parameter a of the hydraulic relation from the calibrated threshold τ.

Finally, in the fourth step, the contributing area, that is, flow accumulation, is propagated according to the D8 flow direction method (O'Callaghan & Mark, 1984), that is, following the steepest direction toward the eight adjacent pixels. The alteration of the contributing area allowed identifying a river network in the UIBs and, therefore, computing the GFI. Given that the UIBs can be characterized by a series of intercluded basins (new smaller UIBs, defined by the dotted lines in Figure 3), steps 2–4 are iteratively repeated as after each iteration the UIBs area reduces progressively thanks to the redefinition of h_r in each UIB.

After the iteration procedure, the threshold binary classification is performed once more to derive the optimal threshold, τ, over the entire area of interest (i.e., examined basin and adjacent UIBs) resulting in a reanalyzed flood hazard map that also accounts for water transfers between basins and UIBs.

3.3 | Hydraulic model

To assess model performances and calibrate the threshold, τ, flood maps were derived from 2D hydraulic simulations and used as reference maps for the GFI-derived flood-prone areas. The unsteady flow simulations were carried out simulating the propagation of the flood in the piedmont area of Castellammare di Stabia.

The hydraulic maps were generated using HEC-RAS 5.0.6 (Hydrologic Engineering Centers—River Analysis System) and based on the same 5-m resolution DEM adopted for the geomorphic analysis. A 2D flow area polygon was drawn and a 2D computational mesh with grid-cell size of 10 m (both DX and DY) and Manning's n value equal to 0.06 was developed. To choose the appropriate cell size, computational time and accuracy were taken into account, while the default Manning's n value was adopted.

First, the reference map for the test basin area was generated. The 2D flow area was connected to boundary condition lines and flow hydrograph and normal depth were selected as boundary conditions for the upstream and downstream lines, respectively. A design hydrograph for a return period of 300 years with a peak flow of about 60 m³/s was used (brown-red line in Figure 4), while the normal depth was set to 0.03. For the validation area, the same design hydrograph was used, carefully rescaled according to the area of the examined basin and its other geomorphic features (i.e., average slope, stream length), obtaining a peak flow of about 12 m³/s (red line marked with squares in Figure 4). In both cases, the computational interval was set to 5 s, while the output interval to 12 min, equal to the simulation time, for a total duration of 6 h. The reference maps obtained correspond to the envelope of the maximum values observed during non-stationary events.

3.4 | Sensitivity analysis

In order to address issues related to flood risk assessment and management in coastal areas, we complemented our analyses by examining the sensitivity of the proposed methodology to the return period in the test basin area. We considered a wide spectrum of flood events return

FIGURE 4 Design hydrographs used as upstream boundary conditions in the two-dimensional hydraulic simulations of the flood propagation in the test and validation areas ($T = 300$ years) and to carry out the sensitivity analysis against the return period in the test area ($T = 2, 5, 10, 20, 30, 50, 100, 200,$ and 300 years)
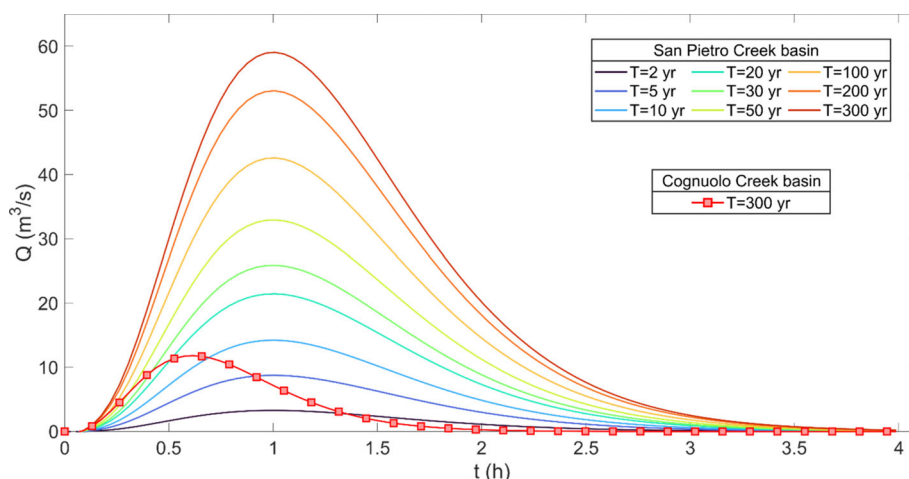
periods ($T = 2, 5, 10, 20, 30, 50, 100, 200,$ and 300 years) and analyzed the dependence of the threshold parameter τ on these values. Different values of τ were considered. These were calibrated by comparing for each return period, T, the GFI-derived flood map with a reference flood map obtained from a 2D hydraulic simulation based on the same model configuration described in the previous subsection. These hydraulic maps correspond to the envelope of the maximum values observed during nonstationary events and were obtained considering design hydrographs with peak flow values of about 3, 9, 14, 21, 26, 33, 43, 53, and 60 m^3/s, respectively (see Figure 4).

For each return period, we also assessed performance metrics in terms of AUC and compared values obtained with the traditional and modified GFI method to highlight the predictive power of the proposed approach.

4 | RESULTS

4.1 | Test area: San Pietro Creek basin

First, the results of the geomorphic analysis based on the application of the traditional GFI method are presented in order to emphasize the limitation of the current method in coastal areas. Figure 5 depicts the GFI and its constituting layers, that is, H and h_r, over the main basin, while a comparison between the GFI-derived flood-prone areas and the reference flood hazard map is shown in Figure 6. From both Figures 5 and 6, it can be noted that river basin boundaries limit the definition of the GFI in the UIBs (yellow features in Figure 6) and, consequently,

interbasins water transfers. A first threshold binary classification was carried out to calibrate the optimal threshold, τ, and an estimated value of $\tau = -0.47$ was obtained. This value was used for the extraction of WD along the watershed divide and the iterative propagation of floodwater until the UIBs area was reduced. Figure 7 shows the reanalyzed flood hazard map, as well as values of the geomorphic flood depth, obtained by performing once more the threshold binary classification over the entire area of interest. Performances of the comparison between the hydraulic map (Figure 6(a)) and the GFI-derived flood hazard maps before (Figure 6(b)) and after (Figure 7) the iteration procedures are summarized in Table 1. In detail, the proposed procedure determined a slight increase in the false positive rate ($R_{FP} = 0.095$), but also a higher true positive rate ($R_{TP} = 0.87$) compared to the traditional GFI method ($R_{FP} = 0.072$ and $R_{TP} = 0.71$). Better performances were also achieved in terms of AUC, whose values increased from 74% before the iteration procedure to 94% after its implementation. Values of AUC refer to the ROC curves depicted in Figure 8. In particular, the ROC curve obtained before the iteration procedure (cyan line) never reaches the upper limit of one because of the presence of undefined values of the GFI in the adjacent areas. It also remains always below the ROC curve obtained through the modified GFI method (blue line).

4.2 | Validation area: Cognuolo Creek basin

The GFI-based geomorphic analysis and the proposed iteration procedure were carried out in the Cognuolo
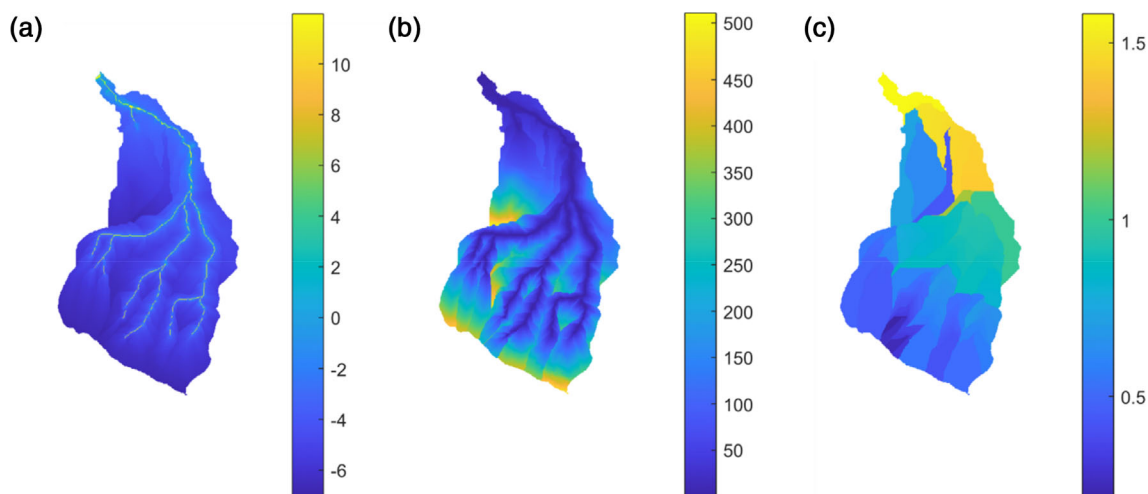

FIGURE 5 Geomorphic analysis on the San Pietro Creek basin using the digital elevation model (DEM) at 5-m resolution: (a) geomorphic flood index (GFI); (b) elevation difference, H; and (c) water level in each cell of the river network, h_r

FIGURE 6 Comparison between the (a) reference flood map used to perform the threshold binary classification and (b) geomorphic flood-prone areas of the San Pietro Creek basin obtained before the implementation of the proposed procedure

Hydraulic flood hazard map (T=300 yr)

GFI flood-prone areas (T=300 yr)

UIBs

San Pietro Creek basin
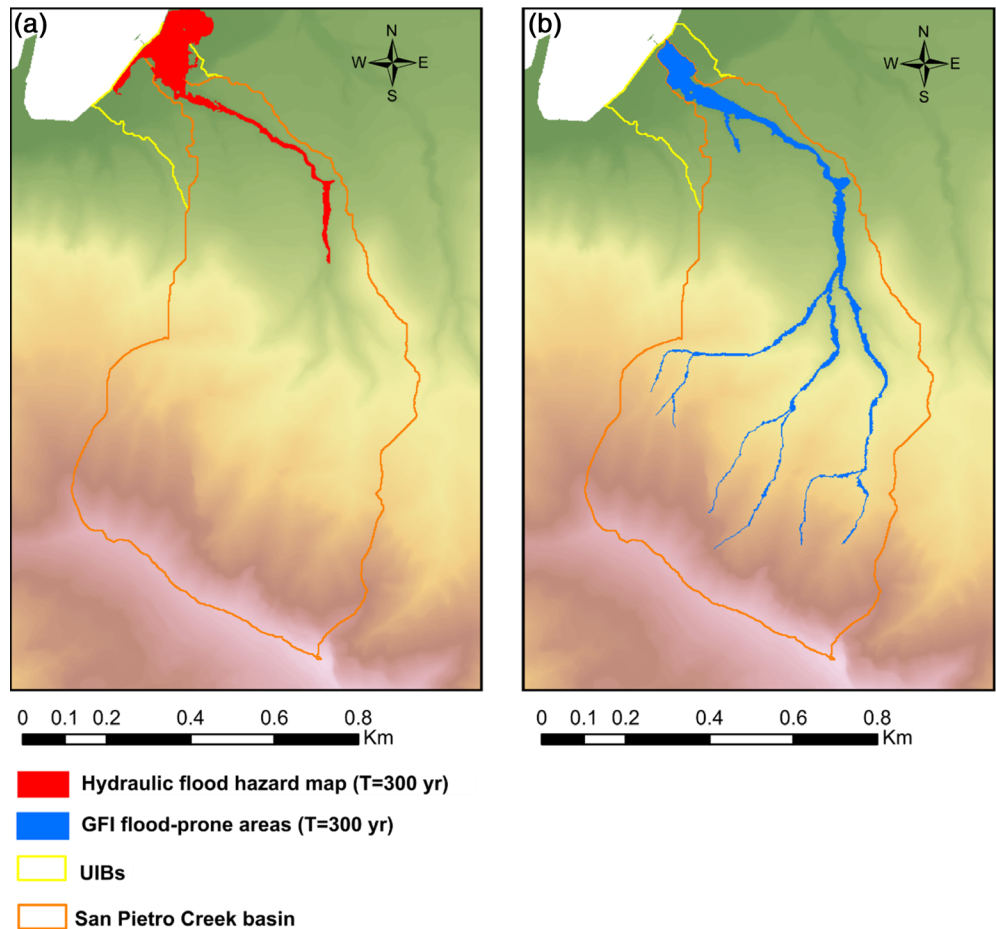
Creek basin and the adjacent UIBs to validate the results of the test area. In this case, no calibration was performed to obtain the optimal threshold, τ, instead the same parameter calibrated for the San Pietro Creek basin was applied to discriminate between flooded and non-flooded areas. A comparison between the GFI-derived flood-prone areas and the reference flood hazard map is shown in Figure 9. Here, an improved prediction of flooded areas using the modified GFI method can be qualitatively observed. These results are supported by the values of the validation statistics computed before and after the iteration procedure and reported in Table 2. Indeed, the methodology leads to an increase in the sensitivity metric ($R_{TP} = 0.79$) and a decrease in the underestimation error ($R_{FN} = 0.21$), compared to performances before the iteration procedure ($R_{TP} = 0.56$ and $R_{TP} = 0.44$). However, a slight increase in the false positive rate, as well as a decrease in the true negative rate can be observed ($R_{FP} = 0.019$ and $R_{TN} = 0.98$ against a value of 0.05 and 0.995, respectively, before the iteration).

4.3 | Sensitivity to the return period

A comprehensive visualization of the results of the sensitivity analysis is given in Figure 10. In detail, the threshold τ shows a general decreasing trend with the increasing return period T. However, sensitivity is limited to flood events with 2- to 20-year return periods (Figure 10(a)). Within this range of events, the relationship between τ and T can be assimilated to a linear function, while τ is constant for larger return periods. Consequently, limited sensitivity to the increased return periods is also observed for the GFI-derived flood-prone areas in the analyzed coastal basin, whose geomorphological features do not lead to significant variations with the increasing flow rate (i.e., increasing magnitude of flood events). These results reflect on the predictive power of the implemented procedure, which was measured in terms of area under the curve. Figure 10(b) demonstrates the need for the proposed method for floods above a certain return period (10-year floods) when interchanges of floodwater occur.

5 | DISCUSSION

In this work, we have further expanded the GFI method by integrating it with an iteration procedure to map flooded areas in rocky coastal zones taking into account the potential water transfer from adjacent basins during flood events. We show that, by simply modifying the map of contributing areas, it is possible to extend flood mapping in the UIBs through the GFI method with improved performances.

The San Pietro Creek basin case study allowed testing the proposed methodology and proved that at-risk areas in the UIBs can be well delineated with a certain degree of accuracy. Results of the iteration procedure were assessed by comparing the GFI-derived flood hazard map and the reference map both qualitatively and quantitatively, by computing performance metrics. Overall, g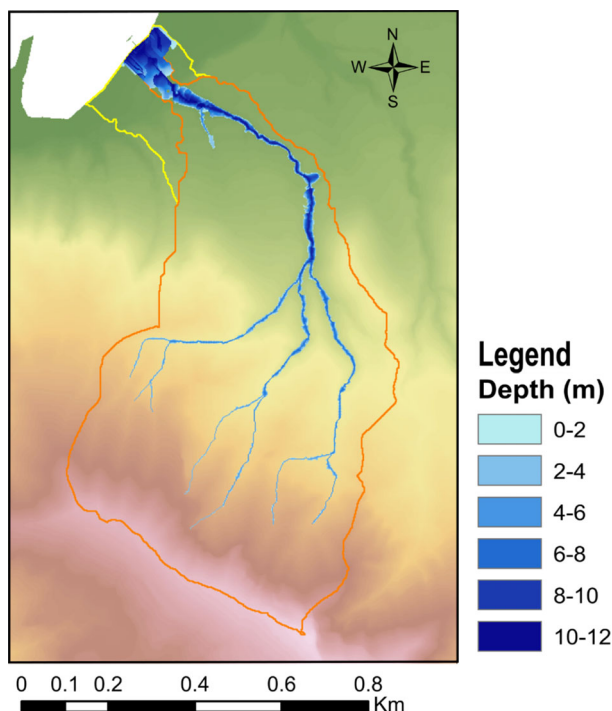ood performances were achieved, as shown by the AUC value of 94%, compared to the traditional GFI method (AUC = 74%). The analysis also proved that τ is a consistent and reliable parameter in predicting flood-susceptible areas. In fact, its value did not change in the two procedures investigated herein: traditional and modified GFI. The fact that τ seems not to be influenced by the introduced iteration procedure suggests that it can be directly applied to the modified GFI without searching for a new optimal value.

In the validation process, the calibrated threshold τ was applied to unstudied areas in the Cognuolo Creek basin, proving τ to be a reliable parameter in delineating flood-prone areas also in the validation case study. The comparison between the reference map and the geomorphic flood hazard maps obtained with the traditional and modified GFI method (which also accounts for interbasin water transfers) showed the ability of a threshold binary classification to detect areas prone to flooding. Validation statistics computed after the iteration procedure showed higher sensitivity ($R_{TP} = 79\%$) and lower underestimation errors ($R_{FN} = 21\%$), compared to the traditional method ($R_{TP} = 56\%$ and $R_{FN} = 44\%$).

Regarding the geomorphic flood depth, WD, we noticed a general overestimation compared with the
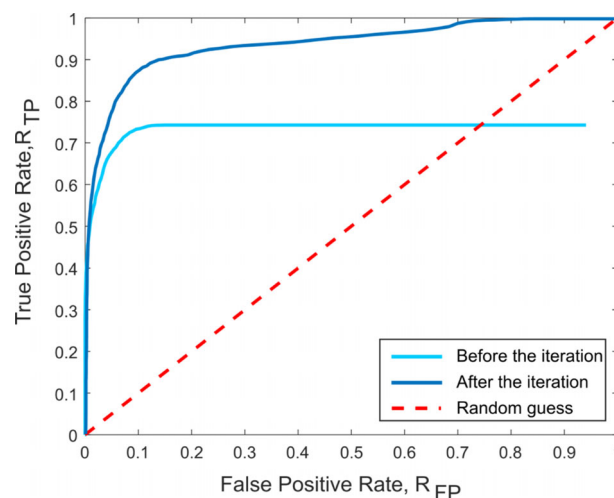

FIGURE 7 Improved geomorphic flood-prone areas ($T = 300$ years) obtained by accounting for interbasin water transfers through the iteration procedure and resulting geomorphic flood depth map for the San Pietro Creek basin

FIGURE 8 Receiver operating characteristics (ROC) curve obtained from the threshold binary classification applied to the San Pietro Creek basin before (cyan line) and after (blue line) the iteration procedure

TABLE 1 Performances of the threshold binary classification implemented at the basin scale (before the iteration) and over the entire study area (after the iteration) in the San Pietro Creek basin case study

	τ	R_{FP}	R_{TP}	$R_{FP} + R_{FN}$	AUC
Before the iteration	−0.470	0.072	0.714	0. 359	0.741
After the iteration	−0.470	0.095	0.868	0.227	0.936

Abbreviation: AUC, area under the curve.

FIGURE 9 (a) Reference flood map used for the validation process in the Cognuolo Creek basin and (b) comparison between the geomorphic flood-prone areas before and after the iteration procedure
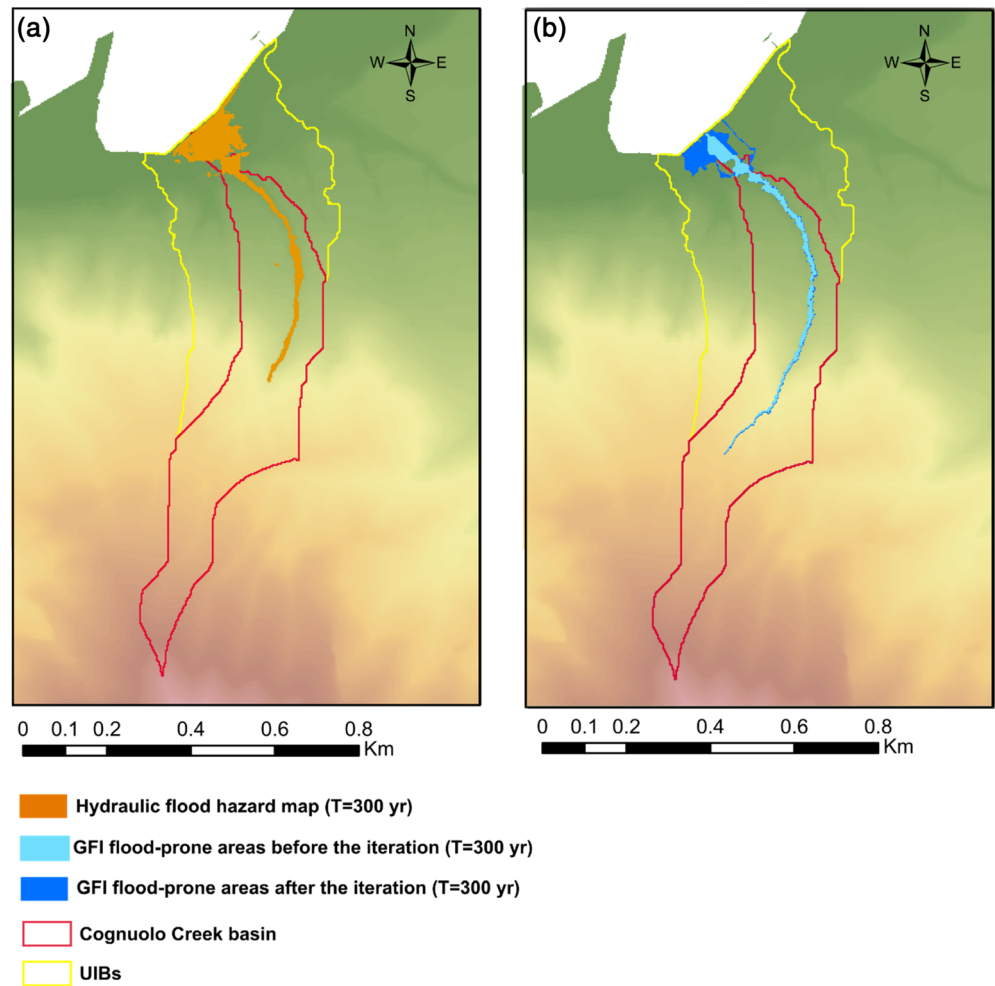
TABLE 2 Performance metrics obtained in the validation process over the Cognuolo Creek basin and computed by comparing the flood reference map and the GFI-derived binary maps obtained before and after the implementation of the proposed iteration procedure, respectively

	τ	R_{FP}	R_{TP}	R_{FN}	R_{TN}
Before the iteration	−0.470	0.005	0.556	0.444	0.995
After the iteration	−0.470	0.019	0.786	0.214	0.981

Abbreviation: GFI, geomorphic flood index.

hydraulic depths. This overestimation is an expected result given the nature of the method that tends to identify the maximum potential flood depth according to the basin morphology, while the hydraulic model provides one of the potential flooding scenarios that depends on the specific flood hydrograph adopted. Moreover, the procedure for the propagation of the flood mapping implemented in this work does not account for hydrodynamic conditions, friction factors or dampening effects, but are only based on the flooding extent. Other factors include the complex geomorphology of the territory under study, characterized by rapid and significant variations in the river flow regime and morphology, which

may require further investigations. Nevertheless, values of WD do not compromise the accuracy of the proposed method the main purpose of which is to assess the tendency of an area to be flooded. The reliability of the method in delineating the extent of floodable areas has been successfully proved in the present work, as well as in previous studies on the topic (Albano et al., 2020; Manfreda & Samela, 2019; Samela et al., 2016, 2017; Tavares da Costa et al., 2019).

The sensitivity analysis against the return period showed that the proposed methodology improves detection of the flood-prone areas in flat-floor valleys, especially when predicting flood extent of extreme events. In
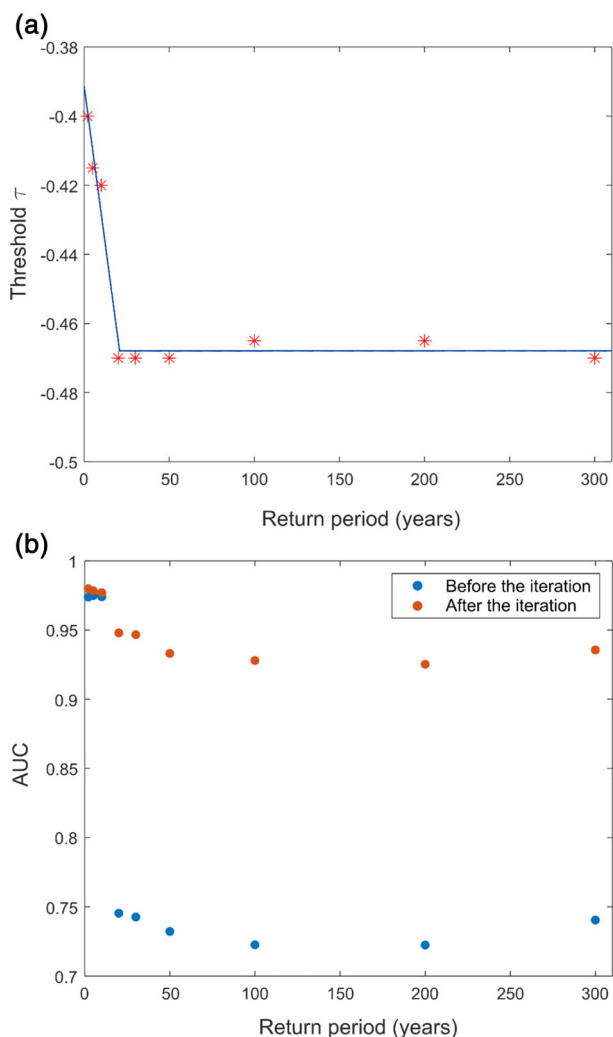
(a)

(b)

FIGURE 10 Results of the sensitivity analysis to the return period. (a) Distribution of the optimal threshold τ and (b) the area under the curve (AUC) for nine return periods

fact, the results proved that, in this case, for flood events with a return period higher than 10 years, a methodology that can capture water transfers between sub-basins is necessary. The performances of such a method (i.e., AUC values) are, indeed, always above those computed with the traditional GFI method.

An additional result of this study is represented by the observed relationship between the threshold τ and the return period of floods. The relationship is shown to be linear up to the return period of 20 years, while after this level the threshold seems to be independent of the return period of the flood event. This may be due to the dynamic and specific nature of the river basin, but it underlines the fact that flood extent changes significantly in the range of lower return periods. Above a specific value, there are relatively minor changes in the extent of flooded areas.

6 | CONCLUSIONS

The overall aim of this work was to propose a DEM-based methodology that further extends the GFI method to map flood risk in small coastal UIBs which are not considered within the traditional GFI procedure, but that can be prone to flooding for events with a return period equal to or greater than 10 years that occur in the larger adjacent basins.

The proposed methodology is particularly suitable for geomorphological settings like those observed in the Sorrentine, Amalfi and Cilento coasts, characterized by rocky coastal areas where several small and steep inter-cluded river basins can be identified along the coastline. The procedure allows for accounting for the interconnection between the subbasins and represents a time- and cost-effective approach for delineating flood-prone areas and mapping flood hazard in coastal basins, where small differences in elevation and slope make it difficult to identify the river network and to apply DEM-based procedures for flood mapping. The procedure proposed in this study was successfully applied to a coastal river basin in Castellammare di Stabia in the Campania region and tested, adopting the same parameterization, in an adjacent river basin.

The study also allowed exploration of the relationship of the threshold parameter with the return period and highlighted a strong dependence for return periods of less than 20 years, while no significant changes in flood extent and therefore threshold parameter were observed for return period higher than 20 years.

The study of coastal basins can be challenging considering the complex nature of such basins (i.e., varying morphology, impulsive and heavy precipitations, and high risk for flooding). This study presents a first attempt to identify an innovative geomorphic procedure to assess flood risk in these areas that can help flood mitigation planning. The methodology requires additional testing and application to new case study areas to further explore limitations and benefits of the method.

DATA AVAILABILITY STATEMENT

Data sharing is not applicable to this article as no new data were created or analyzed in this study.

ORCID

Cinzia Albertini https://orcid.org/0000-0003-3078-3627
Domenico Miglino https://orcid.org/0000-0001-7940-8997
Vito Iacobellis https://orcid.org/0000-0002-8691-8271
Francesco De Paola https://orcid.org/0000-0003-0036-1191
Salvatore Manfreda https://orcid.org/0000-0002-0225-144X

REFERENCES

Albano, R., Samela, C., Crăciun, I., Manfreda, S., Adamowski, J., Sole, A., Sivertun, Å., & Ozunu, A. (2020). Large scale flood risk mapping in data scarce environments: An application for Romania. Water, 12(6), 1834. https://doi.org/10.3390/w12061834

Alfieri, L., Bisselink, B., Dottori, F., Naumann, G., de Roo, A., Salamon, P., Wyser, K., & Feyen, L. (2017). Global projections of river flood risk in a warmer world. Earth's Future, 5(2), 171–182. https://doi.org/10.1002/2016EF000485

Bates, P. D. (2004). Remote sensing and flood inundation modelling. Hydrological Processes, 18(13), 2593–2597. https://doi.org/10.1002/hyp.5649

Bates, P. D., Dawson, R. J., Hall, J. W., Horritt, M. S., Nicholls, R. J., Wicks, J., & Hassan, M. A. A. M. (2005). Simplified two-dimensional numerical modelling of coastal flooding and example applications. Coastal Engineering, 52(9), 793–810. https://doi.org/10.1016/j.coastaleng.2005.06.001

Bhowmik, N. G. (1984). Hydraulic geometry of floodplains. Journal of Hydrology, 68(1), 369–401. https://doi.org/10.1016/0022-1694(84)90221-X

Blöschl, G., Ardoin-Bardin, S., Bonell, M., Dorninger, M., Goodrich, D., Gutknecht, D., Matamoros, D., Merz, B., Shand, P., & Szolgay, J. (2007). At what scales do climate variability and land cover change impact on flooding and low flows? Hydrological Processes, 21(9), 1241–1247. https://doi.org/10.1002/hyp.6669

Degiorgis, M., Gnecco, G., Gorni, S., Roth, G., Sanguineti, M., & Taramasso, A. C. (2012). Classifiers for the detection of flood-prone areas using remote sensed elevation data. Journal of Hydrology, 470–471, 302–315. https://doi.org/10.1016/j.jhydrol.2012.09.006

Degiorgis, M., Gnecco, G., Gorni, S., Roth, G., Sanguineti, M., & Taramasso, A. C. (2013). Flood hazard assessment via threshold binary classifiers: The case study of the Tanaro River basin. Irrigation and Drainage, 62(S2), 1–10. https://doi.org/10.1002/ird.1806

Di Baldassarre, G., Martinez, F., Kalantari, Z., & Viglione, A. (2017). Drought and flood in the Anthropocene: Feedback mechanisms in reservoir operation. Earth System Dynamics, 8(1), 1–9. https://doi.org/10.5194/esd-8-225-2017

Di Baldassarre, G., Viglione, A., Carr, G., Kuil, L., Yan, K., Brandimarte, L., & Blöschl, G. (2015). Debates—Perspectives on socio-hydrology: Capturing feedbacks between physical and social processes. Water Resources Research, 51(6), 4770–4781. https://doi.org/10.1002/2014WR016416

Giannoni, F., Roth, G., & Rudari, R. (2005). A procedure for drainage network identification from geomorphology and its application to the prediction of the hydrologic response. Advances in Water Resources, 28(6), 567–581. https://doi.org/10.1016/j.advwatres.2004.11.013

Hirabayashi, Y., Mahendran, R., Koirala, S., Konoshima, L., Yamazaki, D., Watanabe, S., Kim, H., & Kanae, S. (2013). Global flood risk under climate change. Nature Climate Change, 3(9), 816–821. https://doi.org/10.1038/nclimate1911

Jonkman, S. N. (2005). Global perspectives on loss of human life caused by floods. Natural Hazards, 34(2), 151–175. https://doi.org/10.1007/s11069-004-8891-3

Kirkby, M. J. (1975). Hydrograph modeling strategies. In R. F. Peel, M. D. Chisholm, & P. Haggett (Eds.), Process in physical and human geography (pp. 69–90). Heinemann.

Leopold, L. B., & Maddock, T. (1953). The hydraulic geometry of stream channels and some physiographic implications (Vol. 252). US Government Printing Office.

Manfreda, S., Nardi, F., Samela, C., Grimaldi, S., Taramasso, A. C., Roth, G., & Sole, A. (2014). Investigation on the use of geomorphic approaches for the delineation of flood prone areas. Journal of Hydrology, 517, 863–876. https://doi.org/10.1016/j.jhydrol.2014.06.009

Manfreda, S., & Samela, C. (2019). A digital elevation model based method for a rapid estimation of flood inundation depth. Journal of Flood Risk Management, 12(S1), e12541. https://doi.org/10.1111/jfr3.12541

Manfreda, S., Sole, A., & Fiorentino, M. (2008). Can the basin morphology alone provide an insight into floodplain delineation? WIT Transactions on Ecology and the Environment, 118, 47–56. https://doi.org/10.2495/FRIAR080051

Merz, B., Hall, J., Disse, M., & Schumann, A. (2010). Fluvial flood risk management in a changing world. Natural Hazards and Earth System Sciences, 10(3), 509–527. https://doi.org/10.5194/nhess-10-509-2010

Nardi, F., Grimaldi, S., Santini, M., Petroselli, A., & Ubertini, L. (2008). Hydrogeomorphic properties of simulated drainage patterns using digital elevation models: The flat area issue/Propriétés hydro-géomorphologiques de réseaux de drainage simulés à partir de modèles numériques de terrain: La question des zones planes. Hydrological Sciences Journal, 53(6), 1176–1193. https://doi.org/10.1623/hysj.53.6.1176

Nardi, F., Vivoni, E. R., & Grimaldi, S. (2006). Investigating a floodplain scaling relation using a hydrogeomorphic delineation method. Water Resources Research, 42(9), W09409. https://doi.org/10.1029/2005WR004155

Neumann, B., Vafeidis, A. T., Zimmermann, J., & Nicholls, R. J. (2015). Future coastal population growth and exposure to sea-level rise and coastal flooding—A global assessment. PLoS One, 10(3), e0118571. https://doi.org/10.1371/journal.pone.0118571

Nobre, A. D., Cuartas, L. A., Momo, M. R., Severo, D. L., Pinheiro, A., & Nobre, C. A. (2016). HAND contour: A new proxy predictor of inundation extent. Hydrological Processes, 30(2), 320–333. https://doi.org/10.1002/hyp.10581

O'Callaghan, J. F., & Mark, D. M. (1984). The extraction of drainage networks from digital elevation data. Computer Vision,

Graphics, and Image Processing, 28(3), 323–344. https://doi.org/10.1016/S0734-189X(84)80011-0

Pennetta, M. (2009). Arretramento della linea di riva nel Golfo di Castellammare di Stabia (Na) in risposta all'intercettazione dei sedimenti di deriva litoranea. *Studi Costieri*, 16, 33–50.

Petroselli, A., & Alvarez, A. F. (2012). The flat-area issue in digital elevation models and its consequences for rainfall-runoff modeling. *GIScience & Remote Sensing*, 49(5), 711–734. https://doi.org/10.2747/1548-1603.49.5.711

Samela, C., Albano, R., Sole, A., & Manfreda, S. (2018). A GIS tool for cost-effective delineation of flood-prone areas. *Computers, Environment and Urban Systems*, 70, 43–52. https://doi.org/10.1016/j.compenvurbsys.2018.01.013

Samela, C., Manfreda, S., De Paola, F., Giugni, M., Sole, A., & Fiorentino, M. (2016). DEM-based approaches for the delineation of flood-prone areas in an ungauged basin in Africa. *Journal of Hydrologic Engineering*, 21(2), 6015010. https://doi.org/10.1061/(ASCE)HE.1943-5584.0001272

Samela, C., Troy, T. J., & Manfreda, S. (2017). Geomorphic classifiers for flood-prone areas delineation for data-scarce environments. *Advances in Water Resources*, 102, 13–28. https://doi.org/10.1016/j.advwatres.2017.01.007

Santo, A., Santangelo, N., Beneduce, A., & Iovane, F. (2002). Pericolosità connessa a processi alluvionali in aree pedemontane: Il caso di Castellamare di Stabia in Penisola Sorrentina. *Il Quaternario*, 15(1), 23–37.

Santo, A., Santangelo, N., Di Crescenzo, G., Scorpio, V., Falco, M., & Chirico, G. B. (2015). Flash flood occurrence and magnitude assessment in an alluvial fan context: The October 2011 event in the Southern Apennines. *Natural Hazards*, 78, 417–442. https://doi.org/10.1007/s11069-015-1728-4

Solomon, S., Manning, M., Marquis, M., & Qin, D. (2007). *Climate change 2007—The physical science basis: Working group I contribution to the fourth assessment report of the IPCC* (Vol. 4). Cambridge University Press.

Tavares da Costa, R., Manfreda, S., Luzzi, V., Samela, C., Mazzoli, P., Castellarin, A., & Bagli, S. (2019). A web application for hydrogeomorphic flood hazard mapping. *Environmental Modelling & Software*, 118, 172–186. https://doi.org/10.1016/j.envsoft.2019.04.010

Tavares da Costa, R., Zanardo, S., Bagli, S., Hilberts, A. G. J., Manfreda, S., Samela, C., & Castellarin, A. (2020). Predictive modeling of envelope flood extents using geomorphic and climatic-hydrologic catchment characteristics. *Water Resources Research*, 56(9), e2019WR026453. https://doi.org/10.1029/2019WR026453

Vennari, C., Parise, M., Santangelo, N., & Santo, A. (2016). A database on flash flood events in Campania, southern Italy, with an evaluation of their spatial and temporal distribution. *Natural Hazards and Earth System Sciences*, 16(12), 2485–2500. https://doi.org/10.5194/nhess-16-2485-2016

Violante, C. (2009). Rocky coast: Geological constraints for hazard assessment. *Geological Society, London, Special Publications*, 322(1), 1–31. https://doi.org/10.1144/SP322.1

Wagener, T., Sivapalan, M., Troch, P. A., McGlynn, B. L., Harman, C. J., Gupta, H. V., Kumar, P., Rao, P. S. C., Basu, N. B., & Wilson, J. S. (2010). The future of hydrology: An evolving science for a changing world. *Water Resources Research*, 46(5), W05301. https://doi.org/10.1029/2009WR008906

Wallemacq, P. (2018). *Economic losses, poverty & disasters: 1998–2017*. Centre for Research on the Epidemiology of Disasters, CRED.